

CCN Activity of Isoprene Secondary Organic Aerosol

Gabriella J. Engelhart¹, Richard H. Moore², Athanasios Nenes^{2,3}, Spyros N. Pandis^{1,4,5}

¹Department of Chemical Engineering, Carnegie Mellon University, Pittsburgh, Pennsylvania, USA

²School of Chemical and Biomolecular Engineering, Georgia Institute of Technology, Atlanta, Georgia, USA

³School of Earth and Atmospheric Sciences, Georgia Institute of Technology, Atlanta, Georgia, USA

⁴Department of Chemical Engineering, University of Patras, Patra, Greece

⁵Institute of Chemical Engineering and High Temperatures (ICE-HT), Foundation of Research and Technology (FORTH), Patra, Greece

1.1 Abstract

This work explores the Cloud Condensation Nuclei (CCN) activity of isoprene secondary organic aerosol (SOA), likely a significant source of global organic particulate matter and CCN, produced from the oxidation with OH from HONO/HOOH photolysis in a temperature-controlled SOA chamber. CCN concentrations, activation diameter and droplet growth kinetic information were monitored as a function of supersaturation (from 0.3 to 1.5%) for several hours using a cylindrical continuous-flow streamwise thermal gradient CCN counter connected to a Scanning Mobility Particle Sizer. The initial SOA concentrations ranged from 2-30 $\mu\text{g m}^{-3}$ and presented CCN activity similar to monoterpene SOA with an activation diameter of 35 nm for 1.5% supersaturation and 72 nm for 0.6% supersaturation. The CCN activity improved slightly in some experiments as the SOA aged chemically and did not depend significantly on the level of NO_x during the SOA production. The measured activation diameters correspond to a hygroscopicity parameter, κ , value of 0.12, similar to κ values of 0.1 ± 0.04 reported for monoterpene SOA. Analysis of the water-soluble carbon extracted from filter samples of the SOA suggest that it has a κ of 0.2-0.3 implying an average molar mass between 90 and 150 g mol^{-1} (assuming a zero and 5% surface tension reduction with respect to water, respectively). These findings are

27 consistent with known oxidation products of isoprene. Using threshold droplet growth analysis, the CCN
28 activation kinetics of isoprene SOA was determined to be similar to pure ammonium sulfate aerosol.

29 **1.2 Introduction**

30 Estimates of isoprene emissions are 600 Tg yr^{-1} making it the most abundantly-emitted non-
31 methane hydrocarbon (Guenther et al., 2006). Nevertheless, isoprene has only recently been recognized
32 as a potentially large source of secondary organic aerosol (SOA) despite the relatively high volatility of its
33 first generation oxidation products (Pandis et al., 1991; Edney et al., 2005). The details of the
34 experimental conditions, specifically NO_x levels, presence of a strong acid and temperature, greatly
35 impact the SOA yields, which in recent studies have been as high as 5.5% (Kroll et al., 2006). Aqueous
36 reaction pathways may further increase the yield (Lim et al., 2005).

37 Although laboratory experiments suggest a diverse range in aerosol yield, isoprene SOA has
38 been observed in the atmosphere (Kleindienst et al., 2006; Claeys et al., 2004). Initial global isoprene
39 SOA estimates ranged from 2 Tg yr^{-1} (Claeys et al., 2004) to $10\text{-}120 \text{ Tg yr}^{-1}$ (Matsunaga et al., 2005). Later
40 estimates using the Oslo CTM2 and CAM3-Chem/CLM models ranged between 15 and 19.2 Tg yr^{-1} ,
41 respectively (Hoyle et al., 2007; Heald et al., 2008). Using GEOS-Chem for isoprene SOA, Henze and
42 Seinfeld (2006) estimated a source rate of 6.2 Tg yr^{-1} for isoprene SOA. Farina et al. (2010) incorporated
43 the SOA volatility basis (Donahue et al., 2006) set in GISS II' coupled global simulation and chemical
44 transport model, giving an isoprene SOA production rate of 6.5 Tg yr^{-1} , constituting 22% of the global
45 SOA production.

46 In order to constrain the effect of SOA on clouds, significant effort has been put forth to
47 determine the CCN activity and hygroscopicity of SOA from oxidation of monoterpenes, sesquiterpenes
48 and aromatic volatile organic compounds (Huff Hartz et al., 2005; Varutbangkul et al., 2006; Prenni et

49 al., 2007; Shilling et al., 2007; Engelhart et al., 2008; Asa-Awuku et al., 2009). Regardless of oxidant and
50 experimental conditions, nearly all studies have found SOA to act as “good CCN” under atmospherically-
51 relevant conditions. Atmospheric aging is generally thought to increase the hygroscopicity and CCN
52 activity of SOA (Jimenez et al., 2009), although the formation of oligomers may decrease the particle
53 CCN activity (e.g., VanReken et al., 2005). Asa-Awuku et al. (2010) measured the CCN activity of the
54 water-soluble fraction of SOA (WSOC) from alkenes, monoterpenes, and sesquiterpene parent
55 hydrocarbons, and found it to be remarkably constant and close to that of inorganic salts ($\kappa \approx 0.3$).
56 Köhler Theory Analysis of the samples suggests that shifts in molar mass between samples were
57 accompanied by a compensating change in surface tension depression, thus leading to a relatively
58 constant hygroscopicity parameter. If this finding holds for other SOA systems as well, it implies that the
59 water-soluble fraction of SOA type is the key parameter that controls the value of its hygroscopicity, and
60 offers a physical basis for predictive understanding of SOA hygroscopicity.

61 Another much less constrained aspect of cloud droplet formation is the activation timescale of
62 CCN and variations thereof from changes in composition and particle phase state. Most activation
63 kinetics studies to date focused on potential delays from organics, either because they would form
64 compressed films that affect the uptake rate of water vapor (e.g., Chuang and Feingold, 2001; Nenes et
65 al., 2002), or, slowly dissolve/diffuse, thus requiring more time to activate than deliquesced aerosol
66 (e.g., Shulman et al., 1996; Shantz et al., 2003; Chuang et al., 2006; Asa-Awuku et al., 2007). There is an
67 increasing body of evidence showing that very hygroscopic aerosol (i.e., containing oxidized organics or
68 large amounts of deliquescent material) sampled from a humid environment is associated with rapid
69 activation kinetics (i.e., comparable to that of $(\text{NH}_4)_2\text{SO}_4$ or NaCl aerosol) (e.g., Bougiatioti et al., 2009;
70 Lance et al., 2009; Ruehl et al., 2008, 2009; Padro et al., 2010). Size-resolved ambient CCN
71 measurements have been used to infer the heterogeneity of activation kinetics (Ruehl et al., 2008, 2009)

72 and suggest that the fraction of slowly-activating CCN increases whenever aerosol originates from above
73 the boundary layer. In terms of SOA systems, monoterpene SOA exhibits activation kinetics similar to
74 deliquescent salts (Engelhart et al., 2008); the much less hygroscopic sesquiterpene SOA exhibits slower
75 activation kinetics, that is correlated with the hygroscopicity of the SOA (Asa-Awuku et al., 2009). The
76 activation kinetics of water-soluble aerosol extracted from a wide variety of SOA systems is comparable
77 to that of $(\text{NH}_4)_2\text{SO}_4$ (Asa-Awuku et al., 2010).

78 Despite over a decade of SOA CCN studies, studies focused on isoprene SOA only recently have
79 begun to emerge in the literature. Gunthe et al. (2009) studied the CCN activity of aerosol in the Amazon
80 dominated by biogenic emissions such as isoprene; they found that the hygroscopicity parameter, κ , of
81 the SOA was 0.10 ± 0.03 . King et al. (2010) measured the CCN activity in a continuous flow chamber of
82 seeded isoprene SOA generated with a hydrogen peroxide hydroxyl radical source and found that the
83 CCN activity was largely independent of volatile organic carbon to NO_x ratio. Consistent with Gunthe et
84 al. (2009), the hygroscopicity parameter, κ , of the isoprene SOA was 0.10 ± 0.03 . Similar to the study of
85 Asa-Awuku et al. (2009) (which focused on β -caryophyllene SOA), King et al. (2010) found that the less
86 volatile fraction of the SOA exhibited reduced CCN activity.

87 As important as these findings are for modeling the CCN activity of isoprene SOA, a number of
88 open questions remain. First, the impact of aging on CCN activity of isoprene SOA is not well
89 understood. The effect of NO_x levels and inorganic seed on CCN activity is also unknown; therefore,
90 isolating isoprene SOA for study via homogeneous nucleation of isoprene products is required. It is also
91 important to understand the source of hygroscopicity of the isoprene SOA, by characterizing the CCN
92 properties of the water-soluble fraction of the SOA and unraveling the contributions of solute and
93 surface tension depression effects of the organic. Finally, the droplet activation kinetics of the isoprene
94 SOA remains unconstrained to date. This study focuses on addressing all these questions, by studying

95 the CCN activity, activation kinetics and aging of laboratory-generated SOA from homogeneous
96 nucleation of isoprene oxidation products formed under low- and high-NO_x conditions.

97

98 **1.3 Experimental Methods**

99 1.3.1 SOA Generation

100 Ten experiments (Table 1) were conducted in the Carnegie Mellon University smog chamber,
101 which is a 12 m³ Teflon wall reactor (Welch fluorocarbon) enclosed in a temperature controlled room.
102 The chamber was flushed with dry, particle-free air for several hours prior to each experiment. The
103 experimental setup is shown in Figure 1. Isoprene (Acros Organics, 99+%) was introduced into the
104 chamber via injection through a clean air line. Most experiments were conducted with isoprene
105 injection volumes between 2.5 and 5 μL with the exception of experiment 8 where 19.8 μL were injected
106 for a high concentration experiment. The characteristic mixing time of the chamber is less than 5
107 minutes. Hydroxyl radical was produced via photolysis of nitrous acid (generated by mixing sodium
108 nitrite and sulfuric acid similar to the method described in Ng et al., 2007) and transferred to the smog
109 chamber by clean air through a bubbler. Experiment 1 was conducted under low NO_x conditions,
110 measured at 2 ppb (Table 1). In this experiment hydrogen peroxide (VWR, 50%) was bubbled into the
111 chamber for approximately two hours (Kroll et al., 2006). After stable Proton Transfer Reaction Mass
112 Spectrometer (PTRMS, Ionicon) measurements indicated the chamber was well-mixed, photochemistry
113 was induced by banks of ultra violet black lights with a strong signal around 360 nm located on the walls
114 of the chamber (Presto et al., 2005). For experiments 5-10 (see Table 1) the chamber was pre-cooled to
115 15°C to enhance nucleation. After nucleation, the chamber temperature was gradually warmed to 22°C
116 over the course of 30-60 minutes. In all other experiments the chamber was maintained at 22°C

117 throughout the experiment. In experiments 9 and 10 a second burst of HONO was added after several
118 hours to aging to determine the impact of a dramatic increase in hydroxyl radical concentration on CCN
119 activity. The reported maximum mass concentrations in Table 1 have not been corrected for wall losses
120 and are approximately 10-30% lower than the SOA produced in the corresponding experiment.

121

122 1.3.2 Gas and Particle Composition

123 A Quadrupole Aerosol Mass Spectrometer (Q-AMS, Aerodyne Research, Inc.) was used to
124 monitor aerosol concentration, composition and aerodynamic size (Jayne et al., 2000; Jimenez et al.,
125 2003; Canagaratna et al., 2007). Every 15 seconds the Q-AMS alternated between scanning mass
126 spectrum mode, and, particle time of flight mode. A PTRMS (Ionicon) measured the gas phase
127 concentration of isoprene (m/z 69), some of the major isoprene oxidation products (methacrolein and
128 methyl vinyl ketone, m/z 71), and nitrous acid (m/z 30) (Lindinger, 1998).

129 1.3.3 Cloud Condensation Nuclei Measurement

130 A Differential Mobility Analyzer (DMA, TSI model 3080/3081L) operated at a sheath to aerosol
131 flow ratio of 15:1.5 with a Kr-85 neutralizer (TSI 3077A) ion source was used to scan a range of mobility
132 diameters; the nearly monodisperse classified particle stream was introduced into a Droplet
133 Measurement Technologies Continuous Flow Streamwise Thermal Gradient Chamber Cloud
134 Condensation Nucleus Counter (CCNC; Roberts and Nenes, 2005; Lance et al., 2006) and a Condensation
135 Particle Counter (CPC, TSI model 3772 or model 3010). The CCNC was operated at a sample flow rate of
136 0.5 L min^{-1} and a top-bottom column temperature difference between 4 and 15 K. This combination of
137 instrumentation measured the particle number and the CCN activity as a function of mobility diameter
138 and was merged using Scanning Mobility CCN Analysis (SMCA, Moore et al., 2010) to determine the CCN

139 activated fraction as a function of mobility diameter (the “activation curve”). An additional Scanning
140 Mobility Particle Sizer (SMPS, TSI model 3936) was used as a replicate measurement of the size
141 distribution. A single activation curve was gathered in 2.25 minutes with a 120 second upscan in voltage
142 and a subsequent 15 second downscan. In the course of one experiment up to five supersaturations,
143 ranging from 0.3% to 1.5%, were probed. Data collected during the transient period as the CCNC column
144 temperatures were adjusted (to change supersaturation) was discarded.

145 The CCNC was calibrated using approximately monodisperse ammonium sulfate aerosol
146 following the procedure of Rose et al. (2008) and Engelhart et al. (2008). The CCNC setup during
147 calibration was identical to that used during the experiments (Figure 1) with the substitution of a
148 particle generation system for the reactor. Particle generation was conducted by pushing a 1 g L^{-1}
149 ammonium sulfate solution in pure water via a syringe pump into an atomizer (TSI 3076). The classified
150 particle concentration was maintained below 5000 cm^{-3} by adjusting the flow rate of the syringe pump
151 to avoid coincidence counting errors and supersaturation depletion effects in the CCNC (Lathem and
152 Nenes, in review). Atomized droplets were dried in a silica gel dryer followed by a pressure vent before
153 being sampled by the DMA, CCNC and CPC. SMCA was used to invert the data, align the timing of the
154 CPC and the CCNC, fit the sigmoidal curve and determine the activation diameter, being the diameter
155 for which the normalized activation fraction (i.e., CCN/CN) is equal to 0.5 (e.g., Engelhart et al., 2008;
156 Asa-Awuku et al., 2009; Moore et al., 2010). In cases where the asymptote of the sigmoid is not equal to
157 1 the curve is normalized to one (or viewed another way the 50% activation is found to be half of the
158 total height of the sigmoid). The sigmoidal fit is carried out neglecting the secondary peak located at
159 CCN/CN values below 0.5. Köhler calculations for the effective supersaturation assumed the surface
160 tension and density of water, an effective van't Hoff factor of 2.5 (Gerber et al., 1977; Kumar et al.,

161 2003; Petters and Kreidenweis, 2007; Rose et al., 2008) and the median temperature of the CCNC
162 column.

163

164 1.3.4 WSOC Sampling and Measurement

165 Particles from experiments 5, 6, 7, and 8 were collected on Teflon filters for off-line analysis of
166 the water-soluble organic carbon (WSOC) contained within the SOA. Following a similar procedure to
167 Asa-Awuku et al. (2010) and Padró et al. (2010), the WSOC in the filter samples was extracted in pure
168 water (18 M Ω -cm) during a 1.25 h sonication process with heat (water bath temperature approximately
169 60°C). WSOC concentration was then measured with a Total Organic Carbon (TOC) Turbo Siever
170 analyzer. 3-5 ml of extracted sample was atomized in a collision type atomizer, dried with two
171 diffusional driers and subsequently classified with a scanning mobility particle sizer (TSI SMPS 3080) with
172 a sheath to aerosol ratio of 10:1 L min⁻¹ for analysis by a CPC and a CCNC as described in section 1.3.3.
173 Activation diameters were determined for several supersaturations for a complete characterization of
174 the WSOC CCN activity. The results were then parameterized in terms of their hygroscopicity parameter,
175 and, analyzed to understand the origin of hygroscopicity for the isoprene SOA. Filters from experiments
176 5, 6 and 7 were combined in 60 mL of water to form a filter extract solution containing 1.0 ppmC, and
177 the material from experiment 8 was extracted separately in 60 mL of water to form a solution containing
178 0.6 ppmC. Organic carbon concentrations were comparable to the trace concentrations of Na₂CO₃ and
179 CaCO₃ present in the water measured by ion chromatography. Consequently, the hygroscopicity
180 parameter of the water baseline was determined using the procedure above to be 0.49±0.03 and
181 0.55±0.03 for experiments 5-7 and experiment 8 filter extracts, respectively. The contribution of the
182 water baseline was subtracted from the total κ obtained for the filter extract (since κ , as described in the

183 subsequent section, is additive for mixtures) to determine the hygroscopicity parameter of isoprene
184 WSOC.

185 **1.4 Theoretical Analysis of data**

186 **1.4.1 Hygroscopicity Parameter, κ**

187 Petters and Kreidenweis (2007) proposed a hygroscopicity parameterization, κ , derived from
188 Köhler theory, to parameterize the observed CCN activity of aerosol:

$$189 \quad s(D) = \frac{D^3 - D_d^3}{D^3 - D_d^3(1 - \kappa)} \exp\left(\frac{4\sigma_{s/a}M_w}{RT\rho_w D}\right), \quad (1.1)$$

190 where D is the diameter of the droplet, D_d is the diameter of the dry solute, s is the saturation ratio,
191 $\sigma_{s/a}$ is the surface tension of the solution/air interface, M_w is the molecular weight of water, R is the
192 universal gas constant, ρ_w is the density of water, and T is temperature.

193 For submicron CCN with a substantial soluble fraction, κ can be determined from knowledge of
194 the critical supersaturation and activation diameter of particles as,

$$195 \quad \kappa = \frac{4A}{27d \ln^2 s} \quad (1.2)$$

196 where $A = (4M_w\sigma_w / RT\rho_w)^3$, d is the dry activation diameter, and σ_w is the surface tension of water at
197 the average instrument temperature. For hygroscopic SOA composed of a soluble fraction with volume
198 fraction ε_o , one can show that $\kappa = (M_w/\rho_w)(\rho_o/M_o)(\varepsilon_o/\nu_o)$ where (M_o/ρ_o) is the average molar
199 volume of the organic fraction and ν_o is the effective van't Hoff factor of the soluble organic (Asa-Awuku
200 et al., 2010).

201 For calculation of κ , the organic density was estimated using the method of Kostenidou et al.
202 (2007) “matching” the SMPS and AMS distributions. This method uses the organic aerosol density and
203 the AMS collection efficiency as adjustable parameters to optimize the fit between the volume
204 distribution measured by the SMPS and the mass distribution measured by the AMS. The average
205 estimated AMS collection efficiency was 0.7 for these experiments. The organic density was relatively
206 constant over the course of the experiments at a value of approximately 1.35 g cm^{-3} (Figure 2). This
207 value is within the expected range based upon density estimates of organic aerosol reported in the
208 literature including 1.4 g cm^{-3} for Amazonian ambient sampling (Chen et al., 2009), $1.4\text{-}1.65 \text{ g cm}^{-3}$ for
209 laboratory produced SOA (Kostenidou et al., 2007) and 1.32 g cm^{-3} for organically dominated ambient
210 aerosol (Cross et al., 2007). We will use this estimate of 1.35 g cm^{-3} in this work.

211

212 1.4.2 Droplet activation kinetics

213 When exposed to the same supersaturation profile (that exceeds their critical supersaturation) two
214 CCN will activate and grow to cloud droplets of similar wet diameter, D , provided that their critical
215 supersaturation and mass transfer coefficient of water vapor to the growing droplets is the same. The
216 CCN instrument measures the sizes of droplets at the exit of its growth chamber by an optical particle
217 counter; droplets with sizes larger than $1 \mu\text{m}$ are typically counted as CCN. The droplet size also contains
218 information about the CCN activation kinetics and can be used to relate changes thereof from the
219 presence of organics. In this study, we use approach of Threshold Droplet Growth Analysis (TDGA; Asa-
220 Awuku et al., 2008; 2009; Engelhart et al., 2008; Moore et al., 2008; Bougiatioti et al., 2009; Lance et al.,
221 2009; Sorooshian et al., 2008; Murphy et al., 2009; Asa-Awuku et al., 2010; Padró et al., 2010). TDGA
222 uses a “reference” critical supersaturation - droplet size curve to define the minimum size of droplets

223 that are produced from rapidly-activating CCN (such as $(\text{NH}_4)_2\text{SO}_4$ and NaCl). In this study, we select the
224 wet diameter, D , that corresponds to particles with critical supersaturation equal to the instrument
225 supersaturation (i.e., CCN with a dry diameter equal to the activation diameter, d). If SOA CCN produce
226 droplets that are statistically smaller than the reference at identical critical superaturation (and for
227 identical conditions of instrument operation), they are said to exhibit slower activation kinetics than the
228 reference. If slow activation kinetics is detected, measurements of the CCN size distribution and
229 hygroscopicity can be combined with a numerical model of the instrument to parameterize the
230 activation kinetics (e.g., Asa-Awuku et al., 2009).

231

232 **1.5 Results and Discussion**

233 **1.5.1 Nucleation and SOA Formation**

234 For experiments using HONO, a short delay (of order of a few minutes) preceded the onset of
235 nucleation and growth to sizes detectable by the SMPS at 10 nm. The particles then went through a
236 rapid period of coagulation and growth before forming a stable size distribution which gradually
237 decayed from particle loss to the reaction chamber walls. An example of this process for experiment 4 is
238 shown in Figure 3a. In order to maintain conditions relevant to the atmosphere all but one of these
239 experiments, experiment 8, was conducted at low SOA concentrations $2\text{-}9\ \mu\text{g m}^{-3}$. Experiment 8 was
240 conducted at a higher mass concentration (around $30\ \mu\text{g m}^{-3}$) in order to increase the signal-to-noise
241 ratio in the Q-AMS, and determine whether CCN activity is influenced by the presence of higher volatility
242 compounds in the particle phase. The isoprene concentrations, as measured by m/z 69 on the PTR-MS,
243 were stable before the reaction chamber lights were turned on causing a very rapid decay (Figure 3b).

244 As the isoprene was decaying, the signal related to the isoprene products methacrolein and methyl vinyl
245 ketone (m/z 71) (Warneke et al., 2001) increased sharply, followed by particle number and mass growth.

246 In contrast to the HONO hydroxyl radical source, which produces a fast burst of hydroxyl
247 radicals, the HOOH radical source produces a lower, more sustained hydroxyl radical concentration.
248 Figure 4 highlights the effects of this oxidant precursor change, including a much longer delay before
249 particle formation, incomplete reaction of isoprene precursor gas, and little reaction of the monitored
250 isoprene reaction products.

251

252 1.5.2 CCN Activity of Online SOA

253 In the first stage of the analysis all 2.5 minute activation diameter measurements (collected over
254 several hours) were averaged for a given supersaturation. A typical experiment resulted in
255 measurements of between 25 and 50 activation curves at a single supersaturation. Usually the CCN
256 counter alternated between 4 supersaturations during an experiment. Averaging the activation
257 diameters for each supersaturation for each experiment generated a total of 37 measurements of
258 average, online isoprene SOA CCN activity. The activation diameters were calculated using SMCA for
259 each scan cycle of the DMA during a period of constant supersaturation in the CCNC. Measurements of
260 activation diameters versus supersaturation from all experiments are shown in Figure 5. The CCN
261 activities of the lower and higher SOA concentration experiments were quite similar. This suggests that
262 the higher volatility isoprene SOA products have similar CCN properties as the ones with lower volatility
263 for the concentration range ($2\text{-}30\ \mu\text{g m}^{-3}$) explored in this study.

264 Similar measurements of the CCN activity of the WSOC offline filter samples/extracts (also
265 shown in Figure 5) indicated that the water-soluble fraction is more active than the parent SOA

266 measured online. The CCN activity of the isoprene SOA particles was similar to that of monoterpene SOA
267 (Engelhart et al., 2008) (Figure 5) and significantly more active than β -caryophyllene SOA (Asa-Awuku et
268 al., 2009). Additionally, the CCN activity of particles generated with OH from HOOH (under low NOx
269 conditions) agreed (within the variability of the activation diameter measurements) with those from OH
270 generated with HONO. The CCN activity also seemed to lack a correlation with SOA concentration (not
271 shown), as the activation diameter for the higher mass concentration experiment (experiment 8),
272 agreed to within uncertainty with the lower mass experiment.

273

274 1.5.3 CCN Activity of the water-soluble fraction of SOA

275 Using κ -Köhler theory, the hygroscopicity parameter of the water-soluble SOA was determined
276 to be 0.31 ± 0.03 for the two samples studied, which is in excellent agreement with SOA WSOC
277 measurements of Engelhart et al. (2008), and Asa-Awuku et al. (2009, 2010), suggesting that the water-
278 soluble component of SOA from diverse parent hydrocarbons can be described well using a constant
279 hygroscopicity. The CCN activity of this WSOC is higher than the parent isoprene SOA; given that
280 $\kappa_{SOA} = \kappa_{WSOC} \varepsilon_{WSOC}$, where ε_{WSOC} is the volume fraction of water-soluble organics in the parent SOA
281 (Asa-Awuku et al., 2010), $\kappa_{SOA} \sim 0.1$ (Section 1.1.5) and $\kappa_{WSOC} \sim 0.3$, approximately 30% of the total
282 SOA volume is water-soluble. The activation diameter of isoprene SOA WSOC versus supersaturation, as
283 corrected for the water background, is shown for comparison in Figure 5.

284 This value of κ corresponds to an average molecular weight of $80 \pm 8 \text{ g mol}^{-1}$, assuming the
285 surface tension of water, σ_w , (approximately 0.071 J m^{-2} for the instrument temperatures used in this
286 study) and a van't Hoff factor of 1. This molecular weight is about 50% lower than known low molecular
287 weight oxidation products in isoprene SOA (tetrols and $C_4 - C_5$ dicarboxylic acids with a molecular weight

288 close to 130 g mol^{-1} ; Claeys et al., 2004). One potential explanation for the lower than expected
289 molecular weight inference is the value of surface tension used. If organics depress surface tension (at
290 the point of activation) to a value σ less than σ_w , κ is overestimated by a factor of $(1 - (\sigma_w - \sigma) / \sigma_w)^{-3}$
291 (Asa-Awuku et al., 2010). Too little sample was obtained to facilitate direct surface tension
292 measurements using the pendant drop technique (to determine an upper limit of surface tension
293 depression) or to infer surface depression following the procedure of Asa-Awuku et al. (2008) or Moore
294 et al. (2008). Consequently, we cannot discern the exact contribution of soluble mass and surface
295 tension effects. However, a surface tension depression of 5-10% (in the range inferred for water-soluble
296 organics from other SOA systems; Asa-Awuku 2009,2010; Engelhart et al., 2008) would yield an average
297 molecular weight close to 130 g mol^{-1} and an actual κ between 0.22 and 0.28. Future work will focus on
298 repeating this analysis with sufficient SOA filter to carry out the full analysis.

299

300 1.5.4 Extent of Oxidation and CCN Aging

301 In the Q-AMS, mass to charge (m/z) 44 corresponds to the CO_2^+ ion, which allows it to be used
302 as a proxy measure of extent of oxidation. We calculate the fraction of organics at m/z 44, f_{44} , as the
303 concentration at m/z 44 divided by the total organic aerosol concentration. The fragments at m/z 43 are
304 mostly $\text{C}_2\text{H}_3\text{O}^+$ with some contribution coming from C_3H_7^+ , so f_{43} can give us an indication of moderately
305 oxidized aerosol in our experiments. No Q-AMS data was available for experiment 1.

306 Evidence of aging occurring through hydroxyl radical attack, would manifest in the Q-AMS
307 spectrum as an increase in f_{44} over time. Using this metric, none of the low concentration experiments
308 showed a statistically significant change in extent of oxidation at the 95% confidence level. An indirect
309 expression of aerosol aging is the change in CCN activity over time; many of the experiments showed

310 little evidence of change in the SOA activation diameter for several hours after the formation of the
311 particles. An example is shown in Figure 6, where results from experiment 2 clearly show stable CCN
312 activity and f_{44} over time.

313 While all low mass experiments had a stable f_{44} , low mass experiments 9 and 10 showed a
314 statistically significant decrease in f_{43} . These experiments both had a second burst of hydroxyl radicals
315 from a second addition of HONO later in the experiment, but the decay seems to be linear rather than a
316 step change associated with this HONO addition. Looking at changes in CCN activity for these
317 experiments, all of experiment 10 (Figure 7) and the first portion of experiment 9 (Figure 8) showed a
318 statistically significant decrease in activation diameter at the 99% confidence level in all of the
319 supersaturations measured. Experiment 10 showed a modest decrease in activation diameter with an
320 average decrease of -1.1 nm hr^{-1} for the four supersaturations measured. In contrast to that the first
321 4.25 hours of experiment 9 showed a change in activation diameter with an average decrease of -6.0 nm
322 hr^{-1} for the four supersaturations measured. A change in the slope of the activation diameter versus time
323 line coincided with the addition of a second aliquot of HONO and the activation diameter was steady for
324 the remainder of the experiment (Figure 8). These changes in activation diameter may be related to
325 trends in f_{43} , other spectral changes that could not be elucidated from the Q-AMS, or they could be due
326 to other transformations within the CCN.

327 Since low concentration experiments push the sensitivity limits of the Q-AMS it is possible that
328 noise was masking subtle trends. Experiments with a higher organic aerosol concentration tend to have
329 a reduced amount of noise in f_{44} and f_{43} as compared to their lower organic concentration counterparts.
330 The higher mass experiment 8 (around $30 \mu\text{g m}^{-3}$) did show a small, but statistically significant increase
331 in f_{44} as a function of time (Figure 9). It also showed a corresponding decrease in f_{43} . After the first 0.5

332 hours, when formation and growth of particles is occurring, f_{44} was increasing a rate of 0.08 hr^{-1} and f_{43}
333 was decreasing at a rate of 0.12 hr^{-1} .

334 Since most experiments did not demonstrate an increase in f_{44} , we found the average f_{44} for all
335 experiments in this study to be 0.108 ± 0.028 . Aiken et al. (2008) have shown a significant correlation
336 between f_{44} and O:C for data in Mexico City. Using this fit our average f_{44} can be converted to an O:C of
337 0.45 with an uncertainty from the data of 0.21, which is two standard deviations from the mean.

338 The average f_{44} for this study is right at the threshold of 0.11 that King et al. (2009) has
339 suggested is required to influence CCN activity for α -pinene SOA. Their work showed an abrupt increase
340 in CCN activity for particles with an f_{44} greater than 0.11. Therefore, we carefully examined experiments
341 in this study with f_{44} both above and below this threshold value of 0.11. The highest average f_{44} for a
342 single experiment was 0.13 (experiment 5), which was not discernibly more active as CCN compared to
343 the lowest average f_{44} of 0.08 (experiment 4). In the King et al. (2009) work the f_{44} threshold coincided
344 with a decrease in mass below $1 \mu\text{g m}^{-3}$, which is lower than the masses studied in this work potentially
345 explaining the lack of a relationship between CCN activity and f_{44} for this isoprene SOA system.

346 Overall this study of isoprene SOA aging suggests that as the CCN age their activity remains
347 constant or increases modestly. This is likely not as important as the variation in CCN activity due to
348 initial aerosol composition and size in understanding cloud formation. The hypothesis that the increase
349 in CCN activity is due to aging from increased oxidation is not contradicted by this work. For low mass
350 experiments it is difficult to discern changes in the AMS spectra, but a decrease in the fraction of less
351 oxidized aerosol as measured by f_{43} is apparent. At higher aerosol concentrations both a trend of
352 increasing f_{44} and decreasing f_{43} are observed.

353

354 1.5.5 Hygroscopicity Parameterization

355 The κ value was calculated for each supersaturation measured and all data points are plotted in
356 Figure 10. The low NO_x experiment had an average κ value of 0.14 ± 0.02 , which includes the range of the
357 average κ value for all experiments which was 0.12 ± 0.06 . The water-soluble fraction of oxidation
358 products obtained from the filter extract produced a higher κ value of 0.31 ± 0.03 . We can compare this
359 to the monoterpene work conducted in the same chamber at Carnegie Mellon University which
360 reported κ values between 0.11 and 0.14 for the DMT CCN counter (Engelhart et al., 2008). Additionally,
361 this isoprene SOA work is well within the range reported in the literature for other laboratory generated
362 SOA systems reporting a range of $\kappa = 0.10 \pm 0.04$ (Prenni et al., 2007; Wex et al., 2009) and of ambient
363 measurements of a largely biogenic SOA system where $\kappa_{\text{org}} \approx 0.1$ (Gunthe et al., 2009). As the body of
364 organic CCN literature continues to grow it seems increasingly likely that one κ value may be
365 representative of a broad range of SOA systems.

366

367 1.5.6 Droplet Activation Kinetics

368 In this study, we apply TDGA by comparing the size of droplet formed from SOA particles
369 (measured in the optical particle counter at the exit of the CCN counter column) against the wet size of
370 activated ammonium sulfate CCN with critical supersaturation equal to the instrument supersaturation.
371 The final droplet diameter for the isoprene SOA CCN was at least as large as the ammonium sulfate
372 standard. TDGA was applied to isoprene SOA generated in the chamber (Figure 11) as well as WSOC
373 aerosol generated from filter extracts (not shown). Therefore, we conclude there is no evidence of
374 delays in particle activation as compared to a known inorganic salt.

375 **1.6 Conclusions**

376 The CCN activity of laboratory generated isoprene SOA was studied. The CCN active SOA did not
377 seem to kinetically inhibit the growth of the droplets. The SOA was determined to be moderately
378 oxidized with an f_{44} that was stable within an experiment with an average value of 0.11 ± 0.03 for all
379 experiments. For the majority of experiments the CCN activation diameter showed little or no increase
380 in activity over the course of the experiments. This work finds an average κ value of 0.12 ± 0.06 for the
381 online measurements and 0.31 ± 0.03 for the water-soluble fraction (assuming no surface tension
382 depression due to the organics), which adds to the increasing body of literature finding a similar range of
383 kappa values for a suite of biogenic SOA precursors. These results suggest that approximately 30% of the
384 SOA mass is water-soluble. Furthermore, the κ value for the WSOC is remarkably consistent with the
385 findings of Engelhart et al., (2008) and Asa-Awuku et al. (2009; 2010) who also determined a water-
386 soluble κ value of approximately 0.3 for SOA obtained from alkenes, monoterpenes and sesquiterpene
387 parent hydrocarbons. This suggests that the water-soluble fraction of SOA may be well-characterized
388 using a single hygroscopicity. Finally, the activation kinetics is similar to that of ammonium sulfate. This
389 is consistent with an emerging body of evidence showing that highly oxidized SOA (such as that studied
390 here) does not inhibit the process of water vapor mass transfer from the gas onto the growing droplet
391 population.

392

393 **Acknowledgements**

394 The authors thank M. Trail for ion chromatography analysis and three anonymous reviewers for
395 thorough comments. This work was funded by the U.S. National Science Foundation (ATM-0732598) and
396 the EUCAARI European Union Project.

398 **References**

- 399 Aiken, A. C., P. F. DeCarlo, J. H. Kroll, D. R. Worsnop, J. A. Huffman, K. Docherty, I. M. Ulbrich, C. Mohr, J.
400 R. Kimmel, D. Sueper, Y. Sun, Q. Zhang, A. M. Trimborn, M. J. Northway, P. J. Ziemann, M. R.
401 Canagaratna, M. R. Alfarra, A. S. H. Prevot, J. Duplissy, A. Metzger, U. Baltensperger, and J. L. Jimenez
402 (2008), O/C and OM/OC ratios of primary, secondary, and ambient organic aerosols with high resolution
403 time-of-flight aerosol mass spectrometry, *Environmental Science & Technology*, *42*,
404 doi:10.1021/es703009q.
- 405 Asa-Awuku, A. and A. Nenes (2007), The Effect of solute dissolution kinetics on cloud droplet formation:
406 Extended Köhler Theory, *J. Geophys. Res.*, *112*, D22201, doi:10.1029/2005JD006934.
- 407 Asa-Awuku, A., A. Nenes, A. Sullivan, C. J. Hennigan, and R. J. Weber, (2008) Investigation of molar
408 volume and surfactant characteristics of water-soluble organic compounds in biomass burning aerosol,
409 *Atmos. Chem. Phys.*, *8*, 799-812, doi:10.5194/acp-8-799-2008.
- 410 Asa-Awuku, A., A. Nenes, S. Gao, R. C. Flagan, and J. H. Seinfeld (2010), Water-soluble SOA from Alkene
411 ozonolysis: Composition and droplet activation kinetics inferences from analysis of CCN activity, *Atmos.*
412 *Chem. Phys.*, *10*, 1585–1597, doi:10.5194/acp-10-1585-2010.
- 413 Asa-Awuku, A., G. J. Engelhart, B. H. Lee, S. N. Pandis, and A. Nenes (2009) Relating CCN activity,
414 volatility, and droplet growth kinetics of beta-caryophyllene secondary organic aerosol, *Atmos. Chem.*
415 *Phys.*, *9*, 795–812, doi:10.5194/acp-8-3761-2008.
- 416 Bougiatioti, A., C. Fountoukis, N. Kalivitis, S. N. Pandis, A. Nenes and N. Mihalopoulos (2009) Cloud
417 condensation nuclei measurements in the eastern Mediterranean marine boundary layer: CCN closure
418 and droplet growth kinetics, *Atmospheric Chemistry and Physics*, *9*, 7053 – 7066, doi:10.5194/acp-9-
419 7053-2009.
- 420 Canagaratna, M. R., J. T. Jayne, J. L. Jimenez, J. D. Allan, M. R. Alfarra, Q. Zhang, T. B. Onasch, F.
421 Drewnick, H. Coe, A. M. Middlebrook, A. Delia, L. R. Williams, A. M. Trimborn, M. J. Northway, P. F.
422 DeCarlo, C. E. Kolb, P. Davidovits, and D. R. Worsnop (2007), Chemical and microphysical characterization
423 of ambient aerosols with the Aerodyne aerosol mass spectrometer, *Mass Spectrometry Reviews*, *26*,
424 185-222, doi:10.1002/mas.20115.
- 425 Chen, Q., D. K. Farmer, J. Schneider, S. R. Zorn, C. L. Heald, T. G. Karl, A. Guenther, J. D. Allan, N.
426 Robinson, H. Coe, J. R. Kimmel, T. Pauliquevis, S. Borrmann, U. Pöschl, M. O. Andreae, P. Artaxo, J. L.
427 Jimenez, and S. T. Martin (2009), Mass spectral characterization of submicron biogenic organic particles
428 in the Amazon basin, *Geophys. Res. Lett.*, *36*, L20806, doi:10.1029/2009GL039880.
- 429 Chuang, P.Y. (2006) Sensitivity of cloud condensation nuclei activation processes to kinetic parameters,
430 *J. Geoph. Res.*, *111*, D09201.
- 431 Cross, E. S., J. G. Slowik, P. Davidovits, J. D. Allan, D. R. Worsnop, J. T. Jayne, D. K. Lewis, M. Canagaratna,
432 and T. B. Onasch (2007), Laboratory and ambient particle density determinations using light scattering in

433 conjunction with aerosol mass spectrometry, *Aerosol Sci. Tech.*, 41, 343–359,
434 doi:10.1080/02786820701199736.

435 Claeys, M., B. Graham, G. Vas, W. Wang, R. Vermeylen, V. Pashynska, J. Cafmeyer, P. Guyon, M. O.
436 Andreae, P. Artaxo, and W. Maenhaut, (2004) Formation of secondary organic aerosols through
437 photooxidation of isoprene. *Science*, 303, 1173-1176, doi:10.1126/science.1092805.

438 Dinar, E., I. Taraniuk, E. R. Graber, T. Anttila, T.F. Mentel, and Y. Rudich (2007) Hygroscopic growth of
439 atmospheric and model humic-like substances, *J. Geophys. Res. - A.*, 112, D05211,
440 doi:10.1029/2006JD007442.

441 Dinar, E., I. Taraniuk, E. R. Graber, S. Katsman, T. Moise, T. Anttila, T. F. Mentel, and Y. Rudich, (2006)
442 Cloud Condensation Nuclei properties of model and atmospheric HULIS, *Atmos. Chem. & Phys.*, 6, 2465-
443 2481, doi:10.5194/acpd-6-1073-2006.

444 Donahue, N., A. Robinson, C. Stanier and S. Pandis (2006) Coupled partitioning, dilution, and chemical
445 aging of semivolatile organics, *Environ. Sci. Technol.*, 40 (8), 2635-2643, doi:10.1021/es052297c.

446 Edney, E. O., T. E. Kleindienst, M. Jaoui, M. Lewandowski, J. H. Offenberg, W. Wang, and M. Claeys
447 (2005), Formation of 2-methyl tetrols and 2-methylglyceric acid in secondary organic aerosol from
448 laboratory irradiated isoprene/NO_x/SO₂/air mixtures and their detection in ambient PM_{2.5} samples
449 collected in the eastern United States. *Atmos. Environ.* 39, 5281-5289,
450 doi:10.1016/j.atmosenv.2005.05.031.

451 Engelhart, G. J., A. Asa-Awuku, A. Nenes, and S. N. Pandis (2008) CCN activity and droplet growth
452 kinetics of fresh and aged monoterpene secondary organic aerosol, *Atmos. Chem. Phys.*, 8, 3937-3949,
453 doi:10.5194/acp-8-3937-2008.

454 Farina, S.C., P. J. Adams, S. N. Pandis (2010), Modeling global secondary organic aerosol formation and
455 processing with the volatility basis set: implications for anthropogenic SOA. *Journal Geophys Res.*
456 doi:10.1029/2009JD013046.

457 Gerber, H. E., W. A. Hoppel, and T. A. Wojciechowski (1977), Experimental verification of the theoretical
458 relationship between size and critical supersaturation of salt nuclei, *J. Atmos. Sci.*, 34, 1836–1841,
459 doi:10.1175/1520-0469(1977)034<1836:EVOTTR>2.0.CO;2.

460 Guenther, A., T. Karl, P. Harley, C. Wiedinmyer, P. I. Palmer, and C. Geron (2006) Estimates of global
461 terrestrial isoprene emissions using MEGAN (Model of Emissions of Gases and Aerosols from Nature),
462 *Atmos. Chem. Phys.*, 6, 3181–3210, doi:10.5194/acp-6-3181-2006.

463 Gunthe, S. S., S. M. King, D. Rose, Q. Chen, P. Roldin, D. K. Farmer, J. L. Jimenez, P. Artaxo, M. O.
464 Andreae, S. T. Martin, and U. Pöschl (2009), Cloud condensation nuclei in pristine tropical rainforest air
465 of Amazonia: size-resolved measurements and modeling of atmospheric aerosol composition and CCN
466 activity, *Atmos. Chem. Phys.*, 9, 7551–7575, doi:10.5194/acp-9-7551-2009.

467 Heald, C. L., D. K. Henze, L. W. Horowitz, J. Feddema, J. F. Lamarque, A. Guenther, P. G. Hess, F. Vitt, J. H.
468 Seinfeld, A. H. Goldstein, and I. Fung (2008), Predicted change in global secondary organic aerosol
469 concentrations in response to future climate, emissions, and land use change, *J. Geophys. Res.-Atmos.*,
470 113, D05211, doi:10.1029/2007JD009092.

471 Henze, D. K., and J. H. Seinfeld (2006), Global secondary organic aerosol from isoprene oxidation,
472 *Geophys. Res. Lett.*, 33, L09812, doi:10.1029/2006GL025976.

473 Hoyle, C. R., T. Berntsen, G. Myhre, and I. S. A. Isaksen (2007), Secondary organic aerosol in the global
474 aerosol chemical transport model Oslo CTM2, *Atmos. Chem. Phys.*, 7, 5675–5694, doi:10.5194/acp-7-
475 5675-2007.

476 Huff Hartz, K. E., T. Rosenørn, S. R. Ferchak, T. M. Raymond, M. Bilde, N. M. Donahue, and S. N. Pandis
477 (2005), Cloud condensation nuclei activation of monoterpene and sesquiterpene secondary organic
478 aerosol, *J. Geophys. Res.*, 110, D14208, doi:10.1029/2004JD005754.

479 Solomon, S., D. Qin, M. Manning, Z. Chen, M. Marquis, K. B. Averyt, M. Tignor and H.L. Miller (Eds.)
480 (2007), *IPCC: Climate Change 2007: The Physical Science Basis. Contribution of Working Group I to the*
481 *Fourth Assessment Report of the Intergovernmental Panel on Climate Change*, 996 pp., Cambridge
482 University Press, Cambridge, United Kingdom and New York, NY, USA.

483 Jayne, J. T., D. C. Leard, X. F. Zhang, P. Davidovits, K. A. Smith, C. E. Kolb, and D. R. Worsnop (2000),
484 Development of an aerosol mass spectrometer for size and composition analysis of submicron particles,
485 *Aerosol Science and Technology*, 33, doi:10.1080/027868200410840.

486 Jimenez, J. L., J. T. Jayne, Q. Shi, C. E. Kolb, D. R. Worsnop, I. Yourshaw, J. H. Seinfeld, R. C. Flagan, X.
487 Zhang, K. A. Smith, J. W. Morris, and P. Davidovits (2003), Ambient aerosol sampling using the Aerodyne
488 Aerosol Mass Spectrometer, *Journal of Geophysical Research-Atmospheres*, 108, 8425-8437,
489 doi:10.1029/2001JD001213.

490 Jimenez, J. L., M. R. Canagaratna, N. M. Donahue, A. S. H. Prevot, Q. Zhang, J. H. Kroll, P. F. DeCarlo, J. D.
491 Allan, H. Coe, N. L. Ng, A. C. Aiken, K. S. Docherty, I. M. Ulbrich, A. P. Grieshop, A. L. Robinson, J. Duplissy,
492 J. D. Smith, K. R. Wilson, V. A. Lanz, C. Hueglin, Y. L. Sun, J. Tian, A. Laaksonen, T. Raatikainen, J.
493 Rautiainen, P. Vaattovaara, M. Ehn, M. Kulmala, J. M. Tomlinson, D. R. Collins, M. J. Cubison, E., J.
494 Dunlea, J. A. Huffman, T. B. Onasch, M. R. Alfarra, P. I. Williams, K. Bower, Y. Kondo, J. Schneider, F.
495 Drewnick, S. Borrmann, S. Weimer, K. Demerjian, D. Salcedo, L. Cottrell, R. Griffin, A. Takami, T. Miyoshi,
496 S. Hatakeyama, A. Shimono, J. Y Sun, Y. M. Zhang, K. Dzepina, J. R. Kimmel, D. Sueper, J. T. Jayne, S. C.
497 Herndon, A. M. Trimborn, L. R. Williams, E. C. Wood, A. M. Middlebrook, C. E. Kolb, U. Baltensperger, D.
498 R. Worsnop (2009), Evolution of Organic Aerosols in the Atmosphere, *Science*, 326, 1525-1529,
499 doi:10.1126/science.1180353.

500 King, S. M., T. Rosenørn, J. E. Shilling, Q. Chen, Z. Wang, G. Biskos, K. A. McKinney, U. Pöschl, and S. T.
501 Martin (2010), Cloud droplet activation of mixed organic-sulfate particles produced by the
502 photooxidation of isoprene, *Atmos. Chem. Phys. Discuss.*, 10, 213-244, doi:10.5194/acp-10-3953-2010.

503 King, S. M., T. Rosenørn, J. E. Shilling, Q. Chen, and S. T. Martin (2009), Increased cloud activation
504 potential of secondary organic aerosol for atmospheric mass loadings, *Atmos. Chem. Phys.*, 9, 2959–
505 2971, doi:10.5194/acp-9-2959-2009.

506 Kleindienst, T. E., E. O. Edney, M. Lewandowski, J. H. Offenberg, and M. Jaoui (2006), Secondary organic
507 carbon and aerosol yields from the irradiations of isoprene and R-pinene in the presence of NO_x and SO₂.
508 *Environ. Sci. Technol*, 40, 3807-3812, doi:10.1021/es052446r.

509 Kostenidou, E., R. K. Pathak, and S. N. Pandis (2007), An algorithm for the calculation of secondary
510 organic aerosol density combining AMS and SMPS data. *Aerosol science and technology*, 41, 1002-1010,
511 doi:10.1080/02786820701666270.

512 Kroll, J. H.; N. L. Ng, S. M. Murphy, R. C. Flagan, J. H. Seinfeld (2006), Secondary organic aerosol
513 formation from isoprene photooxidation, *Environ. Sci. Technol.* 40, 1869-1877, doi:10.1021/es0524301.

514 Kumar, P., K. Broekhuizen, and J. P. D. Abbatt (2003), Organic acids as cloud condensation nuclei:
515 Laboratory studies of highly soluble and insoluble species, *Atmos. Chem. Phys.*, 3, 509–520,
516 doi:10.5194/acp-3-509-2003.

517 Lance, S., Medina, J., Smith, J. N., and Nenes, A. (2006) Mapping the operation of the DMT Continuous
518 Flow CCN counter, *Aerosol Sci. & Tech.*, 40, 242-254, doi:10.1080/02786820500543290.

519 Lance, S., A. Nenes, C. Mazzoleni, M. Dubey, H. Gates, V. Varutbangkul, T. A. Rissman, S. M. Murphy, A.
520 Sorooshian, F. Brechtel, R. C. Flagan, J. H. Seinfeld, G. Feingold, and H. Jonsson (2009) CCN Activity,
521 Closure and Droplet Growth Kinetics of Houston Aerosol During the Gulf of Mexico Atmospheric
522 Composition and Climate Study (GoMACCS), *J. Geophys. Res.*, 114, D00F15, doi:10.1029/2008JD011699

523 Lathem, T.L and Nenes, A., Water vapor depletion in the DMT Continuous Flow CCN Chamber: effects on
524 supersaturation and droplet growth, *Aeros.Sci.Tech.*, in review.

525 Lim, H.-J., A. G. Carlton, and B. J. Turpin (2005), Isoprene Forms Secondary Organic Aerosol through
526 Cloud Processing: Model Simulations, *Environ. Sci. Technol.*, 39, 4441–4446, DOI: 10.1021/es048039h.

527 Lindinger, W., A. Hansel, and A. Jordan (1998), On-line monitoring of volatile organic compounds at pptv
528 levels by means of proton-transfer-reaction mass spectrometry (PTR-MS) medical applications, food
529 control and environmental research, *International Journal of Mass Spectrometry and Ion Processes*, 173,
530 191–241, doi:10.1039/a827347z.

531 Matsunaga, S., C. Wiedinmyer, A. B. Guenther, J. J. Orlando, T. Karl, D. W. Toohey, J. P. Greenberg, and
532 Y. Kajii (2005), Isoprene oxidation products are a significant atmospheric aerosol component, *Atmos.*
533 *Chem. Phys. Discuss.*, 5, 11, 143 – 11, 156, doi:10.5194/acpd-5-11143-2005.

534 Moore., R., Nenes, A., and Medina, J. (2010) Scanning Mobility CCN Analysis - A method for fast
535 measurements of size resolved CCN distributions and activation kinetics, *Aeros.Sci.Tech.*, 44, 861-871.
536 Moore, R. H., E. D. Ingall, A. Sorooshian and A. Nenes (2008), Molar mass, surface tension, and droplet
537 growth kinetics of marine organics from measurements of CCN activity, *Geophysical Research Letters*,
538 35, L07801, doi:10.1029/2008GL033350.

539 Murphy, S. M., H. Agrawal, A. Sorooshian, L. T. Padró, H. Gates, S. Hersey, W. A. Welch, H. Jung, J. W.
540 Miller, D. R. Cocker III, A. Nenes, H. H. Jonsson, R. C. Flagan and J. H. Seinfeld (2009), Comprehensive
541 simultaneous shipboard and airborne characterization of exhaust from a modern container ship at sea,
542 *Environmental Science & Technology*, doi:10.1021/es802413j.

543 Ng, N. L., P. S. Chhabra, A. W. H. Chan, J. D. Surratt, J. H. Kroll, A. J. Kwan, D. C. McCabe, P. O. Wennberg,
544 A. Sorooshian, S. M. Murphy, N. F. Dalleska, R. C. Flagan, and J. H. Seinfeld (2007), Effect of NO_x level on
545 secondary organic aerosol (SOA) formation from the photooxidation of terpenes, *Atmos. Chem. Phys.*, 7,
546 5159–5174, doi:10.5194/acp-7-5159-2007.

547 Padró, L. T., A. Asa-Awuku, R. Morisson, and A. Nenes (2007), Inferring Thermodynamic Properties from
548 CCN Activation Experiments: Single-component and Binary Aerosols, *Atmos. Chem. & Phys.*, 7, 5263-
549 5274, doi:10.5194/acp-7-5263-2007.

550 Padró, L.T., D. Tkacik, T. Lathem, C. J. Hennigan, A. P. Sullivan, R. J. Weber, L. G. Huey, and A. Nenes
551 (2010), Investigation of CCN relevant properties and droplet growth kinetics of water-soluble aerosol
552 fraction in Mexico City, *J. Geoph. Res.*, 115, D09204, doi:10.1029/2009JD013195.

553 Pandis, S. N., S. E. Paulson, J. H. Seinfeld, and R. C. Flagan (1991), Aerosol formation in the
554 photooxidation of isoprene and β -pinene, *Atmos. Environ.*, 25A, 997–1008, doi:10.1016/0960-
555 1686(91)90141-S.

556 Petters, M. D. and S. M. Kreidenweis (2007), A single parameter representation of hygroscopic growth
557 and cloud condensation nucleus activity, *Atmos. Chem. Phys.*, 7, 1961–1971, doi:10.5194/acp-7-1961-
558 2007.

559 Prenni, A.J., M.D. Petters, S.M. Kreidenweis, P.J. DeMott, and P.J. Ziemann (2007), Cloud droplet
560 activation of secondary organic aerosol, *Journal of Geophysical Research*, 112, D10223,
561 doi:10.1029/2006JD007963.

562 Presto, A. A., K. E. Huff Hartz, and N. M. Donahue (2005), Secondary Organic Aerosol Production from
563 Terpene Ozonolysis. 1. Effect of UV Radiation. *Environ. Sci. Technol.*, 39, pp 7036–7045, DOI:
564 10.1021/es050174m.

565 Roberts, G. C., and A. Nenes (2005), A continuous-flow streamwise thermal-gradient CCN chamber for
566 atmospheric measurements, *Aerosol Sci. & Tech.*, 39, 206–221, doi:10.1080/027868290913988.

567 Rose, D., S. S. Gunthe, E. Mikhailov, G. P. Frank, U. Dusek, M. O. Andreae, and U. Pöschl (2008),
568 Calibration and measurement uncertainties of a continuous-flow cloud condensation nuclei counter
569 (DMT-CCNC): CCN activation of ammonium sulfate and sodium chloride aerosol particles in theory and
570 experiment. *Atmos. Chem. Phys.*, 8, 1153–1179, doi:10.5194/acp-8-1153-2008.

571 Shantz, N. C., W. R. Leitch, and P. Caffrey (2003), Effect of organics of low solubility on the growth rate
572 of cloud droplets., *J. Geophys. Res.*, 108, 4168, doi:10.1029/2002JD002540.

573 Shilling, J. E., S. M. King, M. Mochida, and S. T. Martin (2007), Mass spectral evidence that small changes
574 in composition caused by oxidative aging processes alter aerosol CCN properties, *J. Phys. Chem.*, 111,
575 3358–3368, doi:10.1021/jp068822r.

576 Shulman, M. L., M. C. Jacobson, R. J. Carlson, R. E. Synovec, and T. E. Young (1996), Dissolution behavior
577 and surface tension effects of organic compounds in nucleating cloud droplets, *Geophys. Res. Lett.*, 23,
578 277–280, doi:10.1029/95GL03810.

579 Sorooshian, A., S. M. Murphy, S. Hersey, H. Gates, L. T. Padro, A. Nenes, F. J. Brechtel, H. Jonsson, R. C.
580 Flagan, and J. H. Seinfeld (2008), Comprehensive airborne characterization of aerosol from a major
581 bovine source, *Atmos. Chem. Phys.*, 8, 5489–5520, doi:10.5194/acp-8-5489-2008.

582 Surratt, J. D., J. H. Kroll, T. E. Kleindienst, E. O. Edney, M. Claeys, A. Sorooshian, N. L. Ng, J. H. Offenberg,
583 M. Lewandowski, M. Jaoui, R. C. Flagan, and J. H. Seinfeld (2007), Evidence for Organosulfates in
584 Secondary Organic Aerosol, *Environmental Science & Technology*, *41*, 517-527, doi:10.1021/es062081q.

585 VanReken, T. M., N. L. Ng, R. C. Flagan, and J. H. Seinfeld (2005), Cloud condensation nucleus activation
586 properties of biogenic secondary organic aerosol, *J. Geophys. Res.*, *110*, d07206,
587 doi:10.1029/2004JD005465.

588 Varutbangkul, V., F. J. Brechtel, R. Bahreini, N. L. Ng, M. D. Keywood, J. H. Kroll, R. C. Flagan, J. H.
589 Seinfeld, A. Lee, and A. H. Goldstein (2006), Hygroscopicity of secondary organic aerosols formed by
590 oxidation of cycloalkenes, monoterpenes, sesquiterpenes, and related compounds, *Atmos. Chem. Phys.*,
591 *6*, 2367–2388, doi:10.5194/acp-6-2367-2006.

592 Warneke, C., R. Holzinger, A. Hansel, A. Jordan, W. Lindinger, U. Pöschl, J. Williams, P. Hoor, H. Fischer,
593 P. J. Crutzen, H. A. Scheeren and J. Lelieveld (2001), Isoprene and Its Oxidation Products Methyl Vinyl
594 Ketone, Methacrolein, and Isoprene Related Peroxides Measured Online over the Tropical Rain Forest of
595 Surinam in March 1998, *Journal of Atmospheric Chemistry*, *38*, 167-185, doi:10.1023/A:1006326802432.

596 Wex, H., M. D. Petters, C. M. Carrico, E. Hallbauer, A. Massling, G. R. McMeeking, L. Poulain, Z. Wu, S. M.
597 Kreidenweis, and F. Stratmann (2009), Towards closing the gap between hygroscopic growth and
598 activation for secondary organic aerosol: Part 1 - Evidence from measurements, *Atmos. Chem. Phys.*, *9*,
599 3987–3997, doi:10.5194/acpd-9-955-2009.

600

601

602

603

Table 1: Experiments carried out in isoprene SOA study

Experiment No.	Isoprene initial (ppb)	Max SOA Formed ($\mu\text{g m}^{-3}$)	Max Particle Number* 10^{-3} (cm^{-3})	AMS f_{44} ^a	Filter	Precool	NO _x initial (ppb)
1 ^b	89	2	9.1	-	no	no	2 ^c
2	61	4	870	0.11	no	no	1000
3	120	5	770	0.11	no	no	950
4	115	8	860	0.08	no	no	1050
5	75	3	580	0.13	yes	yes	750
6	58	3	670	0.13	yes	yes	900
7	56	4	510	0.11	yes	yes	900
8	260	30	1100	0.09	yes	yes	900
9 ^d	64	9	790	0.11	no	yes	500
10 ^d	83	7	620	0.1	no	yes	650

604

605

606 ^a $f_{44} = [m/z 44] (\mu\text{g m}^{-3}) / C_{\text{OA}} (\mu\text{g m}^{-3})$, C_{OA} is the mass concentration of the total organic aerosol607 ^bExperiment under low NO_x conditions with hydrogen peroxide as hydroxyl radical precursor608 ^cBelow instrument detection level609 ^dAdditional HONO added later in experiment

610

611

612

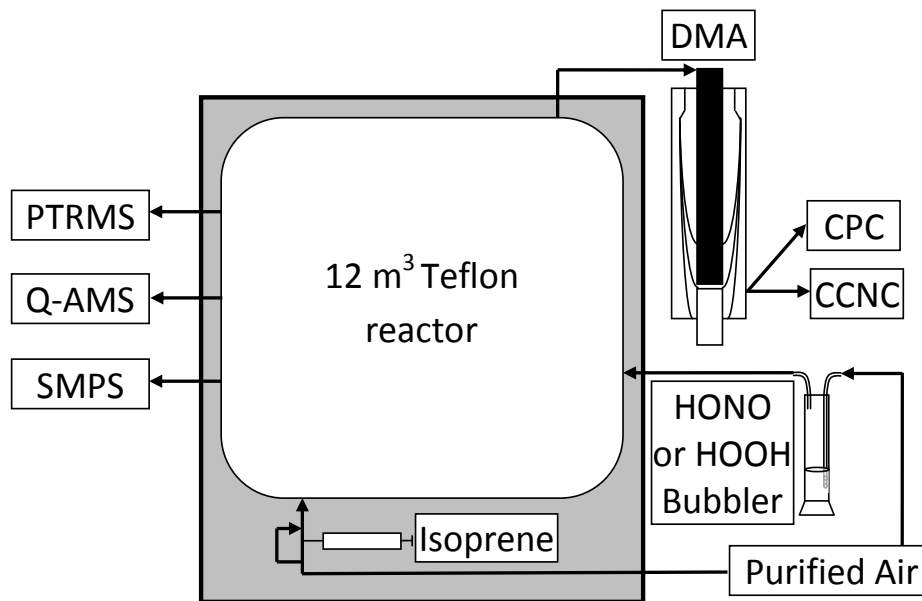
613

614

615

616

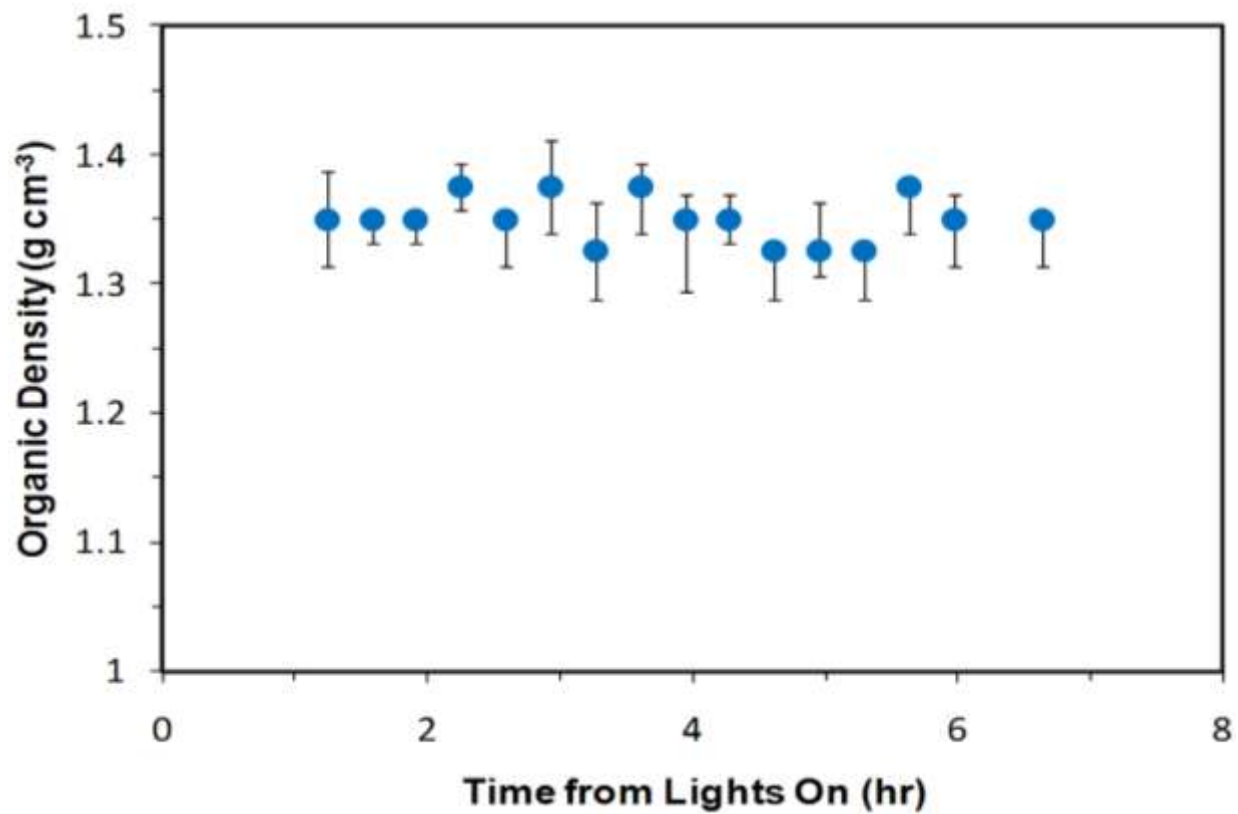
617



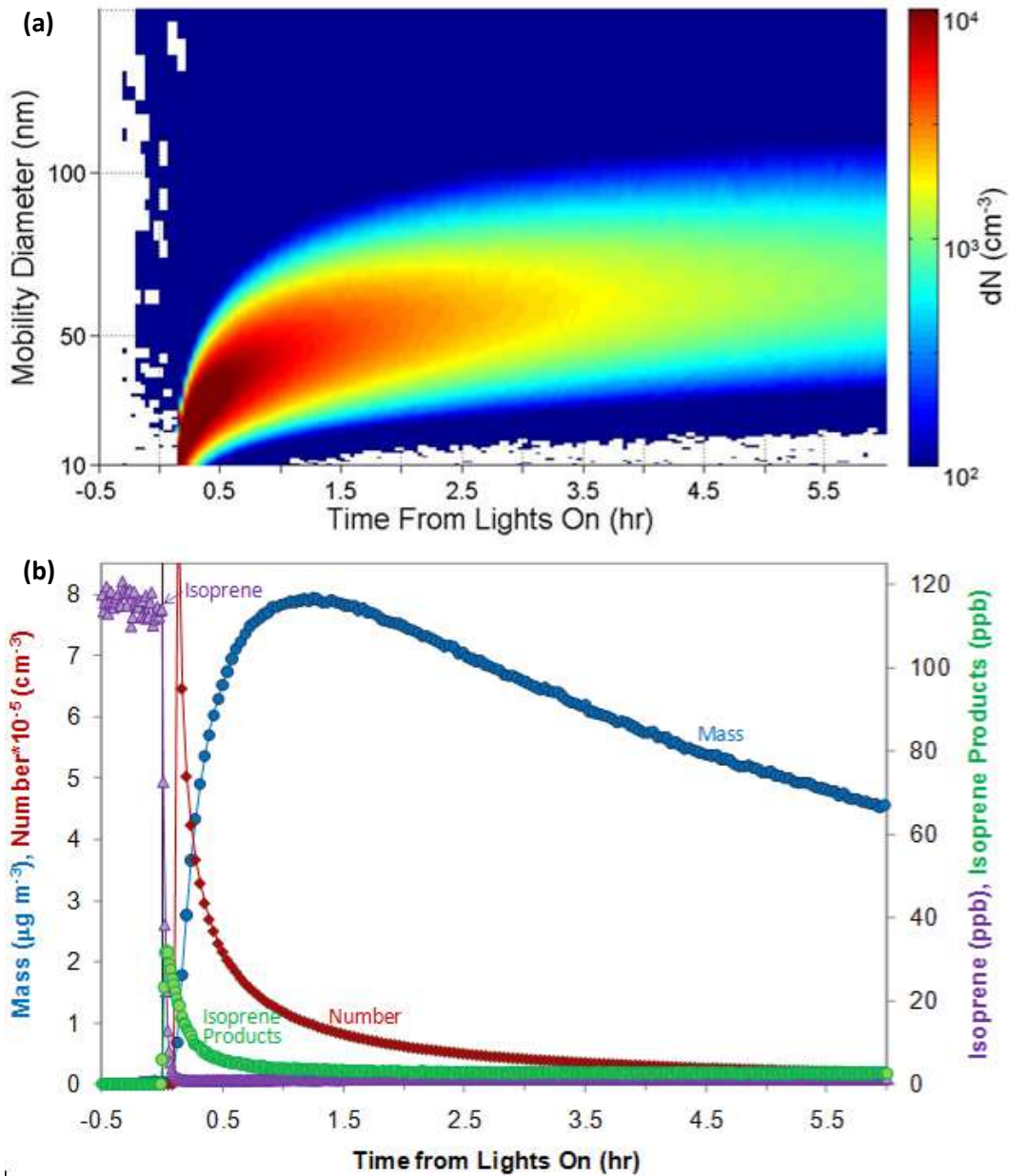
618
619
620
621
622
623
624

Figure 1: Experimental setup discussed in Section 1.3.

625
626

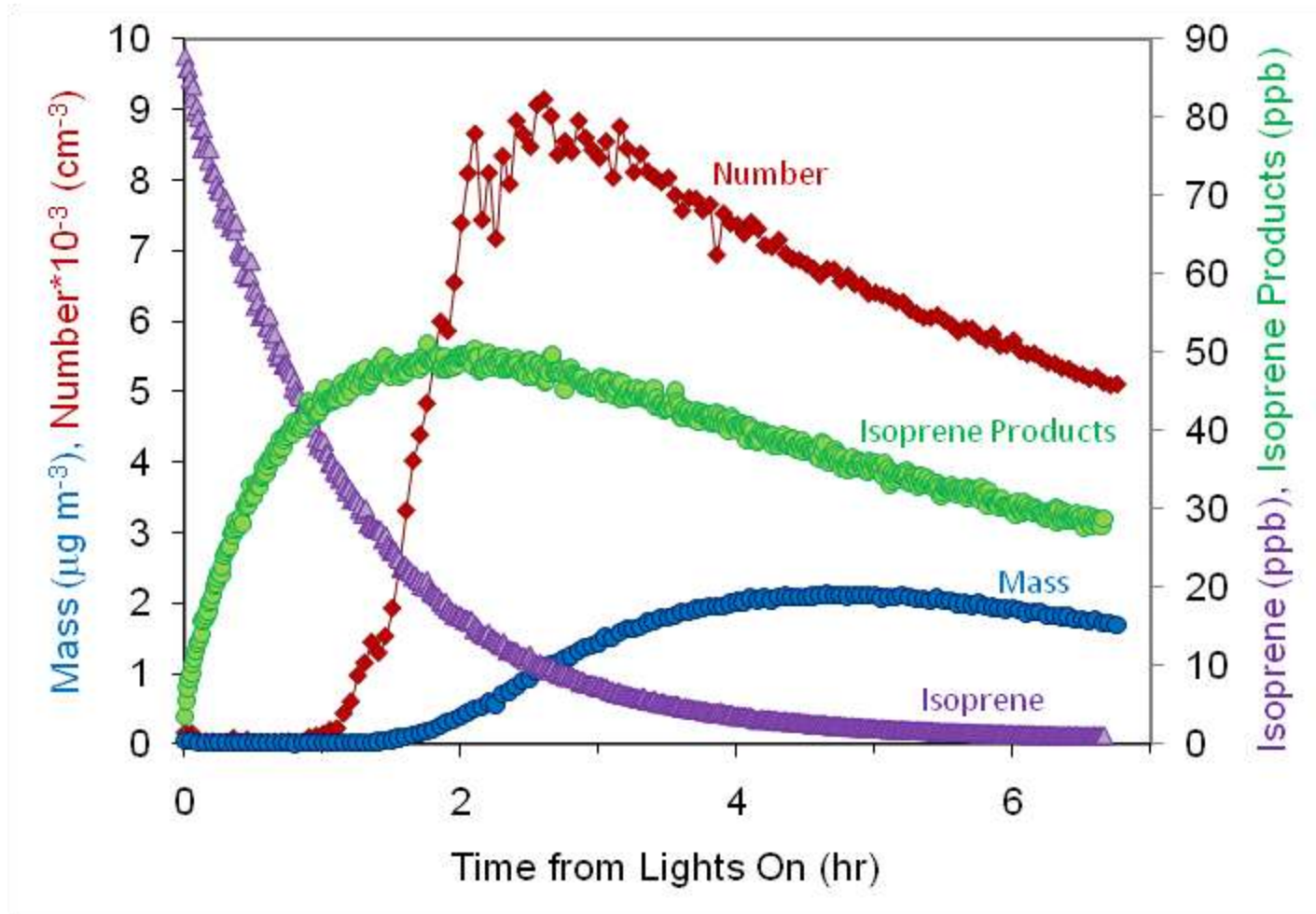


627
628
629 Figure 2: Time from lights on versus organic density as calculated by comparing SMPS mobility diameter
630 distributions to Q-AMS aerodynamic diameter distributions for experiment 2.



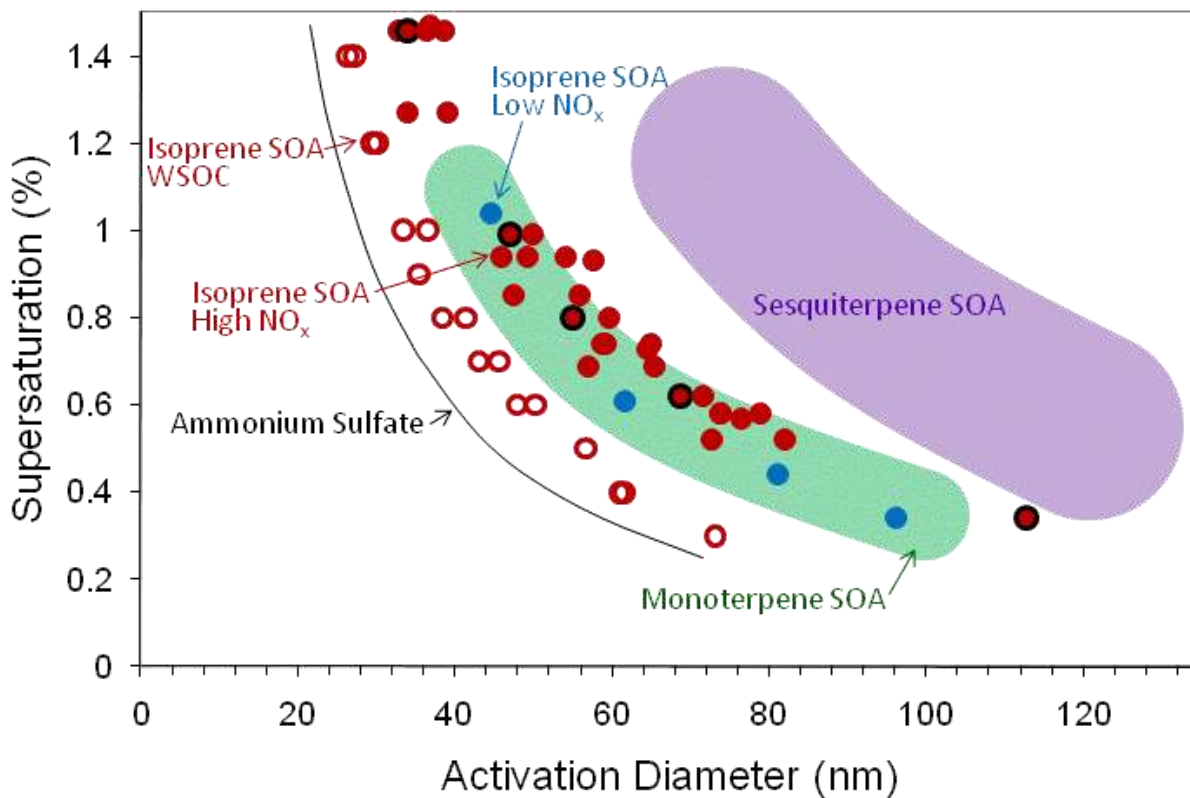
631
 632
 633
 634
 635
 636
 637

Figure 3: Details from experiment 4. **(a)** SMPS mobility diameter as a function of time from lights on. The colors indicate the intensity of the particle concentration from 10^2 to 10^4 cm^{-3} . **(b)** Time from lights on versus SMPS mass (blue circles), SMPS number (red diamonds), isoprene concentration as measured by m/z 69 (purple triangles) and concentration of isoprene products as measured by m/z 71 (green circles).



638
 639
 640
 641
 642
 643
 644
 645
 646

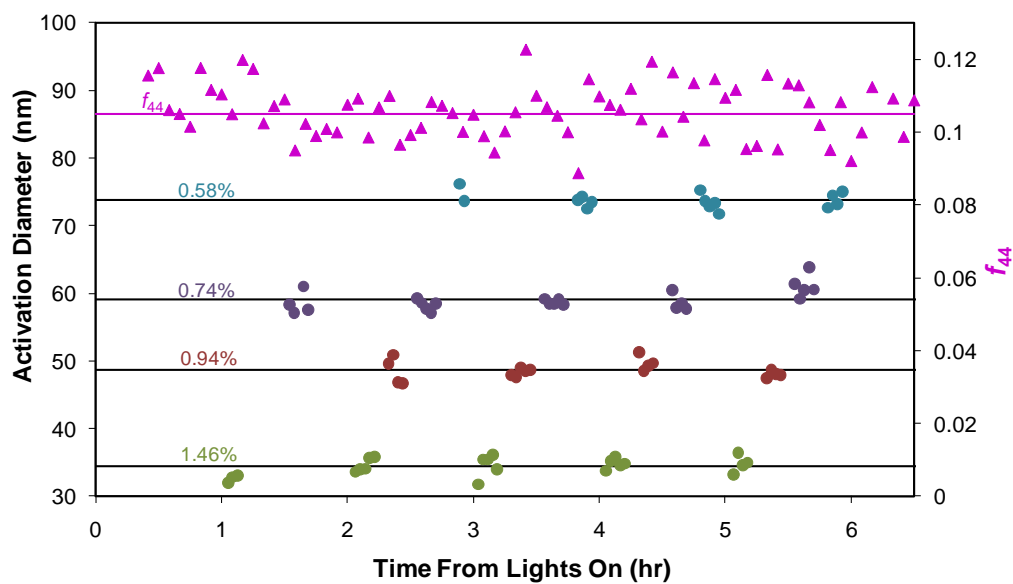
Figure 4: Time from lights on versus SMPS mass (blue circles), SMPS number (red diamonds), isoprene concentration (purple triangles) and concentration of isoprene products (green circles) for experiment 1 (hydrogen peroxide as the hydroxyl radical source).



647
 648
 649
 650 Figure 5: Activation diameter versus percent supersaturation for nine high NO_x isoprene SOA
 651 experiments (shown in solid red) and one low NO_x isoprene SOA experiment shown in blue (experiment
 652 1 in Table 1). Data from the high mass loading experiment (experiment 8 in Table 1) are outlined in
 653 black. Offline filter measurements of isoprene SOA WSOC activity are shown as unfilled red circles.
 654 Regions of monoterpene SOA (green) and β-caryophyllene SOA (purple) from previous studies are
 655 highlighted for reference. Ammonium sulfate is shown in black.
 656

657
 658

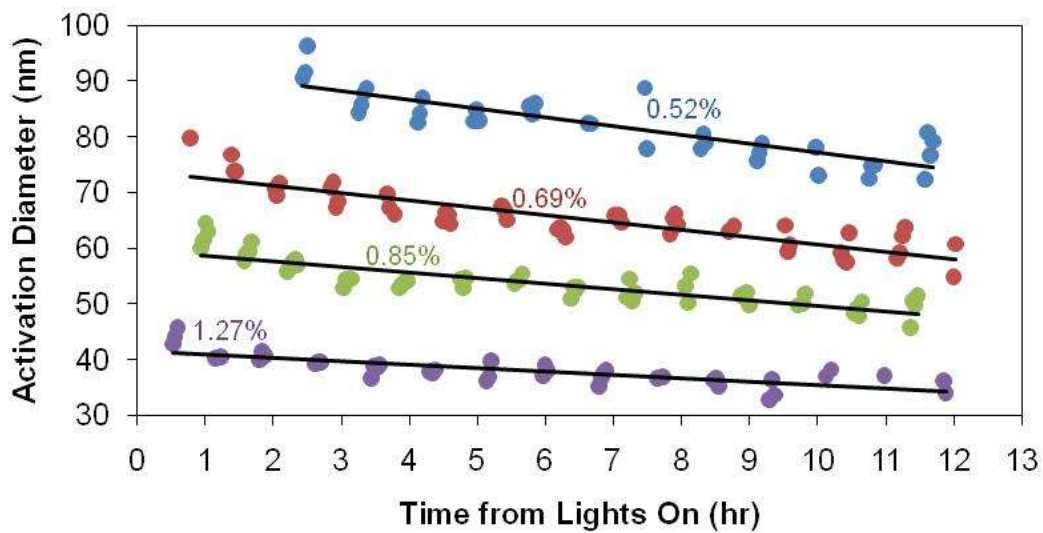
659



660
661
662
663
664
665
666
667
668

Figure 6: Time from lights on versus CCN activation diameter and fraction m/z 44 for experiment 2. Average activation diameters for each supersaturation as shown as black lines. Average f_{44} is shown as a magenta line.

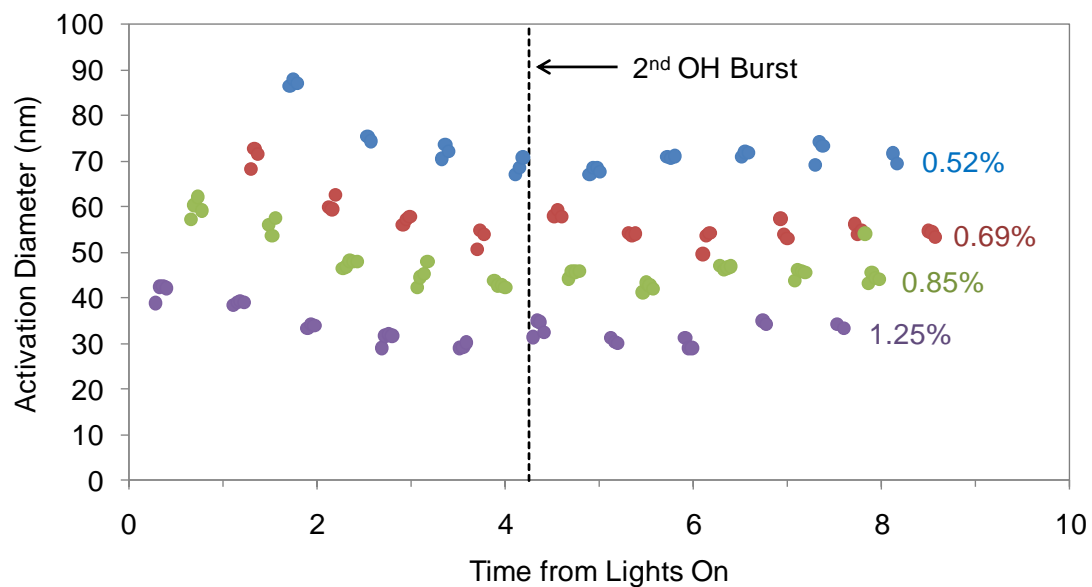
669



670
671
672
673
674
675

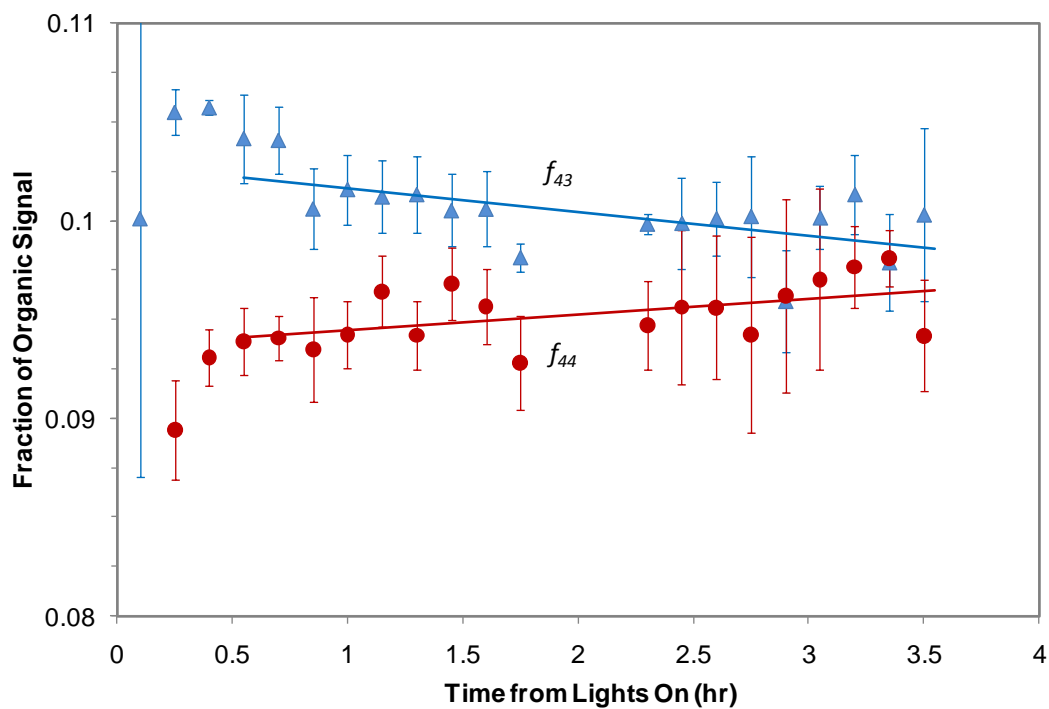
Figure 7: Time from lights on versus CCN activation diameter for experiment 10. The black lines are trendlines for each supersaturation.

676



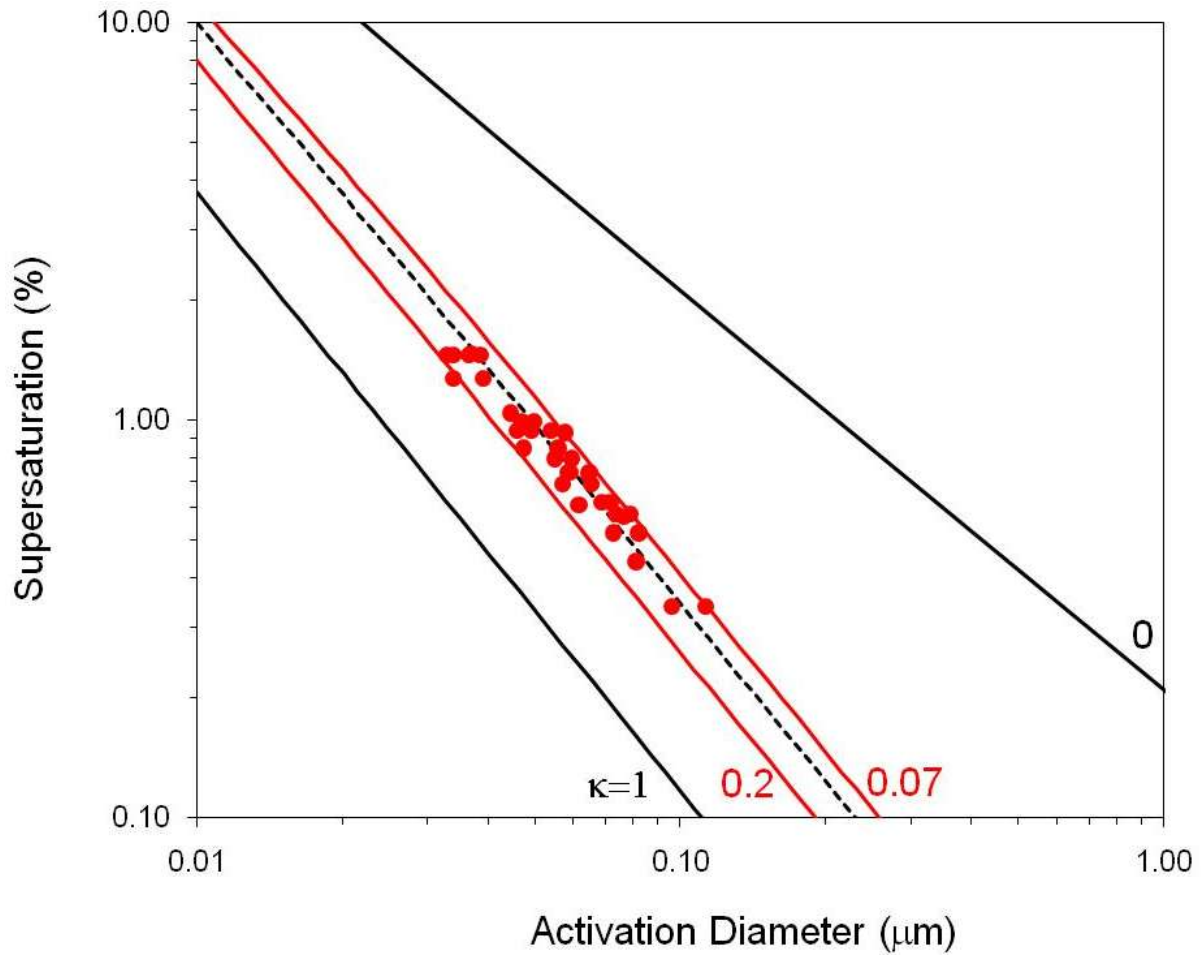
677
678
679
680
681
682
683
684
685

Figure 8: Time from lights on versus CCN activation diameter for experiment 9. The dashed line indicates the second hydroxyl radical burst upon illumination of a second aliquot of HONO.



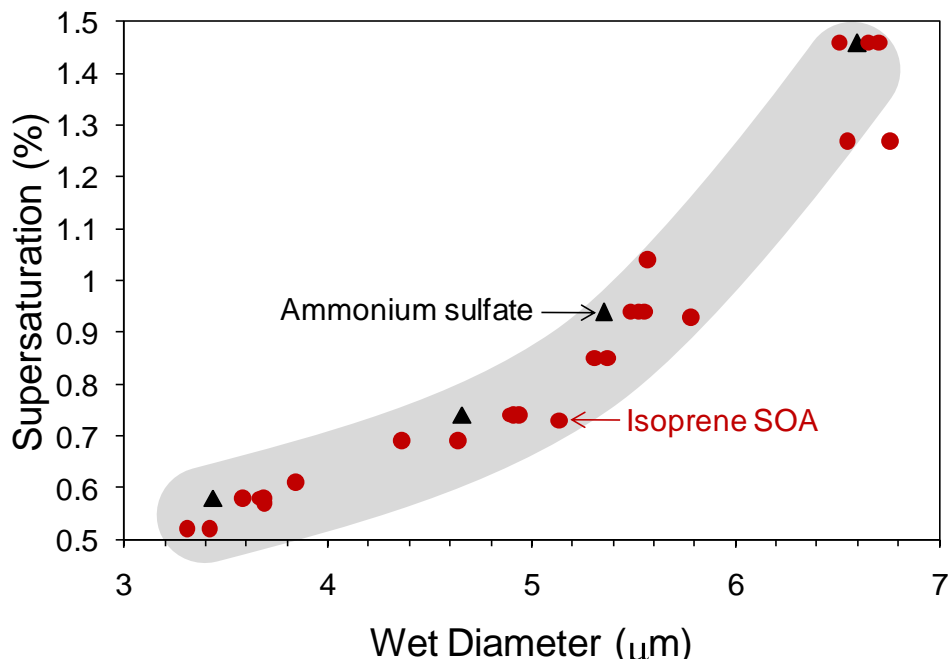
686
687
688
689

690 Figure 9: Time from lights on versus f_{44} (red circles) and f_{43} (blue triangles) for experiment 8. There is a
691 slight increase in f_{44} and a decrease in f_{43} over the course of the experiment with some initial transient
692 effects as the organic aerosol is nucleating and growing. The red and blue lines are trend lines of the
693 data after 0.5 hours.



694
 695
 696
 697
 698
 699
 700
 701
 702
 703
 704
 705

Figure 10: Activation diameter versus supersaturation. Each point represents the average of the measurements at that supersaturation in each experiment. All but one experimental point lie within the region bounded by kappa equals 0.07 and 0.2, shown in red. The black, dashed line indicates the average κ value for all experiments, 0.12. Lines of $\kappa=0$ (wetting by pure water) and 1 (very active) are also shown.



706
707
708
709
710
711
712

Figure 11: Droplet wet diameter versus percent supersaturation. Isoprene SOA particles are shown as red circles and ammonium sulfate particles are shown as black triangles. The gray region highlights a range of wet diameters versus supersaturation.